A probabilistic model for on-line estimation of the GNSS carrier-to-noise ratio

Hamza Issa, Georges Stienne, Serge Reboul, Maximilian Semmling, Mohamad Raad, Ghaleb Faour, Jens Wickert

Available online at www.sciencedirect.com

ScienceDirect

Signal Processing 00 (2020) 1–20

www.elsevier.com/locate/procedia

A probabilistic model for on-line estimation of the GNSS carrier-to-noise ratio

Hamza Issa[a,b,*], Georges Stienne[a], Serge Reboul[a], Maximilian Semmling[c], Mohamad Raad[d], Ghaleb Faour[b], Jens Wickert[c,e]

[a] *Laboratory d'Informatique Signal et Image de la Côte d'Opale (LISIC),Université du Littoral Côte d'Opale (ULCO), Calais, France*
[b] *National Council of Scientific Research (CNRS-L), Remote Sensing Research Center, Mansouriyeh, Lebanon*
[c] *German Research Centre for Geosciences (GFZ), Potsdam, Germany*
[d] *Department of Engineering, Lebanese International University (LIU), Beirut, Lebanon.*
[e] *Technische Universität Berlin (TUB), Germany*

Abstract

This article is dedicated to the estimation of the GNSS signal carrier-to-noise ratio using the in-phase component of the signals as observations. In a GNSS receiver, it is the statistic of the correlation provided by the code tracking loop that is used to estimate the carrier-to-noise ratio. In fact, carrier-to-noise estimation is used to monitor the performance of GNSS receivers and the quality of the received signals. In this article, we aim at high rate carrier-to-noise estimation, namely the code repetition rate (e.g. 1ms for GPS C/A), in order to maximize the time resolution of carrier-to-noise observations. We show that in a 1-bit quantization receiver, the in-phase component of the signal can provide a direct observation of the signal amplitude, and therefore of the carrier-to-noise ratio. However, the model that links the 1ms rate observations of the in-phase component with the signal amplitude is non-linear. The non-linear expression that links the maximum value of the in-phase correlation component to the signal amplitude is derived. In order to estimate the time varying amplitudes of the signals, we propose an Extended Kalman Filter to reverse the non-linear expression with the noisy observations of correlation provided by the tracking loop. The proposed model and filter inversion method are assessed on synthetic and real data, while investigating the effect of the cross-correlation contribution of the visible satellites on the estimations. We show using real data that, for a 1-bit quantization receiver, the proposed estimator can achieve the same accuracy as a widely known commercial GNSS receiver with a much higher data rate. We also show that the proposed approach can cope with abrupt changes in the observations compared to a classical C/N_0 estimate.

.

Keywords: GNSS, amplitude estimation, non-linear filtering, C/N_0 estimation

1. Introduction

Telecommunication systems use the power of the received signal, normalized by the noise power, as an indicator of the quality of reception. The Signal-to-Noise Ratio (SNR) is called Carrier-to-Noise Ratio

*Corresponding author.
Email addresses: hamza.issa@univ-littoral.fr (Hamza Issa), georges.stienne@univ-littoral.fr (Georges Stienne), serge.reboul@univ-littoral.fr (Serge Reboul)

(C/N_0) when the noise power is defined for a unit of bandwidth. Measurements of C/N_0 are often used in global navigation satellite system (GNSS) applications to monitor the receiver processing and its response to noisy environments [1, 2], determine whether the code and carrier tracking loops are in lock, and to detect the signal-to-noise environment in order to predict the performance of the receiver [3]. High rate variations in the C/N_0 are associated with multipath disturbances [4] and low rate variations with indoor or in forest positioning [5]. In this regard, C/N_0 observations have been used for remote sensing applications by the GNSS-Reflectometry (GNSS-R) community. In this context, the C/N_0 of the GNSS signals received on Earth directly from the GNSS satellites as well as after reflection on the Earth surface are compared to retrieve some geophysical parameters of the reflective surface such as its height, shape or soil moisture [6, 7, 8, 9].

The carrier-to-noise ratio is used to observe the amplitude of a GNSS signal. However, this amplitude can't be directly estimated because the GNSS antenna perceives a combination of all the GNSS signals from the satellites in view, which results in mixing the received signals. In this context, the inversion of the antenna measurements to retrieve the C/N_0 of the signals from each satellite in view is an ill posed problem. However, each GNSS satellite signal can be differentiated with its Code Division Multiple Access (CDMA) code [10]. The C/N_0 of the received signals can, therefore, be derived from the demultiplexing and demodulation processes [11]. In fact, each received signal can be expressed as a sum of a sine function and a cosine function (i.e. 90 degrees out of phase). The sine part is denoted as the in-phase component I and the cosine part as the quadrature component Q of the signal. The stages of demodulation and demultiplexing are realized respectively with a Phase Lock Loop (PLL) and a Delay Lock Loop (DLL) providing the in-phase component I and quadrature component Q measurements for each satellite. It can be shown that I are noisy observations of the signal amplitude and Q are observations of the noise [12]. In the classical approach, the statistics of these two components are used to estimate the SNR, which is proportional to the signal amplitude. Finally C/N_0 is derived by the product of the SNR with the noise equivalent bandwidth of the receiver RF (Radio Frequency) front end.

In practice, the difficulty associated to the estimation of the C/N_0 is the derivation of the statistical parameters of the two components in quadrature. This estimation process assumes that the noise is stationary and the signal amplitude is constant. This assumption is less restrictive for high rate estimations. However, the accuracy of the estimation depends on the duration of the observation. In this context, accuracy and estimation rate are two ambivalent parameters.

Several estimates of C/N_0 have been proposed for GNSS applications in order to maximize the accuracy with minimal implementation complexity. The most widely used estimate is the Standard Estimate (SE) also referred to as Narrow-to-Wideband power ratio estimate [12]. This estimate uses the accumulated I and Q samples from the prompt P correlator [13]. Another way to measure C/N_0 using the accumulated in-phase and quadrature components from the prompt correlator is the Correlator Comparison method. Unfortunately, these estimators perform poorly with weak signal and high interference environment [13]. Norman C. Beaulieu has also introduced an intuitively motivated algorithm to measure C/N_0 using the accumulated I and Q samples from the prompt P correlator [14]. This method achieves high accuracy with minimum complexity, but requires a relatively high integration time to acheive the desired accuracy. The moment-based estimator is the most accurate SNR estimate and is shown to achieve the Cramer-Rao Lower Bound but this estimate has a high complexity cost [15]. It also needs a long integration time in order to achieve a good accuracy. Other data-aided estimates presuppose a knowledge of the transmitted data symbols which is a common assumption in GNSS applications. In this regard, the Maximum Likelihood Estimate (MLE) outperforms other estimators under the assumption of known data bits, because it provides a good compromise in term of complexity and accuracy [16]. Several versions of this estimate have been proposed with [16] or without [17] perfect phase synchronization and for modern GNSS signals that have pilot and data channels [18].

In a classical GNSS receiver, 1-bit or 2-bit quantization are used. However, in some military applica-

tions, 8 bits are necessary to accurately process the Power Spectral Density (PSD) of the signal in order to prevent GNSS spoofing. We developed for this work, a bit grabber to record the data with 1-bit or 2-bit quantization in collaboration with a GNSS specialized firm called Syntony. The DLL, PLL and FLL estimate the parameters of the signal in our self-built 1-bit GNSS software receiver. In fact, signal digitalization is done off-line but the software receiver processes the data on-line. The on-line loops correct the phase delay error, the code delay error and the error in Doppler during the tracking process. As a result, accurate estimates of the GNSS signal parameters are obtained. The tracking error increases when the SNR of the signal decreases, but this error is low and not significant given the noise power on I. Eventually, both errors (tracking and noise errors) are included in the value of the C/N_0. We show in a preceding work [19], that we can indeed reach centimeter precise position estimates every 1ms. In that case, observations of phase and Doppler were used to process the code delay of the GNSS signal obtained every 1ms. In fact, increasing the quantization bits will improve the estimate accuracy of I (the in-phase component of the signal). However, the observations will be dependent on the automatic gain control (AGC). Moreover, the noise power on the observation of I is too high to observe this improvement.

In the context of this work, a probabilistic model of the front end architecture of a coherent detector is proposed. Coherent detectors are used in several applications like GNSS, telecommunication systems, radar systems, and sensors (Dual-Phase Lock-In Amplifier). Concerning the GNSS applications, the minimum length of integration T_b (1ms code period for GPS C/A) is known and is an objective in our development. Furthermore, several parameters render the model complex and show the interest of the proposed statistical approach. In our model, we indeed take into account the cross correlation between the different satellites. We also take into account the receiver-satellite velocity in the carrier frequency. The model in the context of this application shows different complexities that can be included in the probabilistic model of a coherent detector.

In this article, we show that for 1-bit quantization in a digital receiver, the digitized signals are independent of the automatic gain control, and thus the mean value of the in-phase component I, provides a direct observation of the signal amplitude and therefore of C/N_0. We estimate the carrier-to-noise ratio at high rate (1 ms rate for GPS C/A) using 1 ms rate observations of I. For example, high rate C/N_0 estimation is essential in multipath, and dynamic GNSS-R applications, where the C/N_0 estimation rate determines the system's ability to cope with the rapid displacement of the GNSS receiver and defines the rate at which the environment can be analyzed. However, the model that links the signal amplitude to the 1ms rate observations of I is non-linear and we derive its expression. For linear models, the Kalman filter, being a recursive filter, produces state estimates that are optimal in the minimum mean-squared error (MMSE) sense [20]. However, since the measurement equations are non-linear, we propose an on-line estimate of the amplitudes of the signals based on an Extended Kalman Filter (EKF) that uses measurements of I as observations. The linearization of the measurement equation that links I to the signal amplitude is then derived.

Based on the foregoing, this article is organized as follows: Section II presents the GNSS front end processing and the one bit front end model. In the third section, an on-line estimate of the signal amplitude in the form of an EKF is introduced, while interpreting the non-linear expression that links the observations of I to the amplitudes of the signals. The linearization of the measurement equation is derived in the fourth section. In the fifth section, the proposed methodology is assessed using both synthetic and real data. Finally, conclusions are provided in the sixth section.

2. GNSS front end

2.1. GNSS front end processing

The purpose of the RF front end is to provide digital signal samples to the signal processing block. The signals $s^r(t)$ sensed by the GNSS antenna are amplified using a Low Noise Amplifier (LNA) due to the fact that the signals are immersed in noise. The LNA is characterized by its gain and noise figure [21]. Then,

the amplitudes of the signals are regulated using an automatic gain control (AGC). After that, the received signals are down converted with a local oscillator frequency f_{LO} to an intermediate frequency f_{IF}. Consider the following GPS C/A signal $s(t)$ after down conversion to an intermediate frequency f_{IF}:

$$s(t) = \sum_{l \in V} K\, A_l(t) CA_l(t + \tau_l) \sin(2\pi f_l\, t + \phi_l) + K\, \eta(t) \tag{1}$$

Where V is the set of visible satellites. $A_l(t)$ is the amplitude of the signal, $CA_l(t)$ is the CDMA code of satellite l and τ_l is the code delay. f_l and ϕ_l are respectively the frequency and the phase delay of the carrier. f_l^D is the Doppler frequency associated to satellite l with $f_l = f_{IF} + f_l^D$. $\eta(t)$ is a zero mean additive Gaussian noise with a unit variance and K the Gain of the AGC. A scheme of the RF front end of a GNSS receiver is depicted in figure 1.

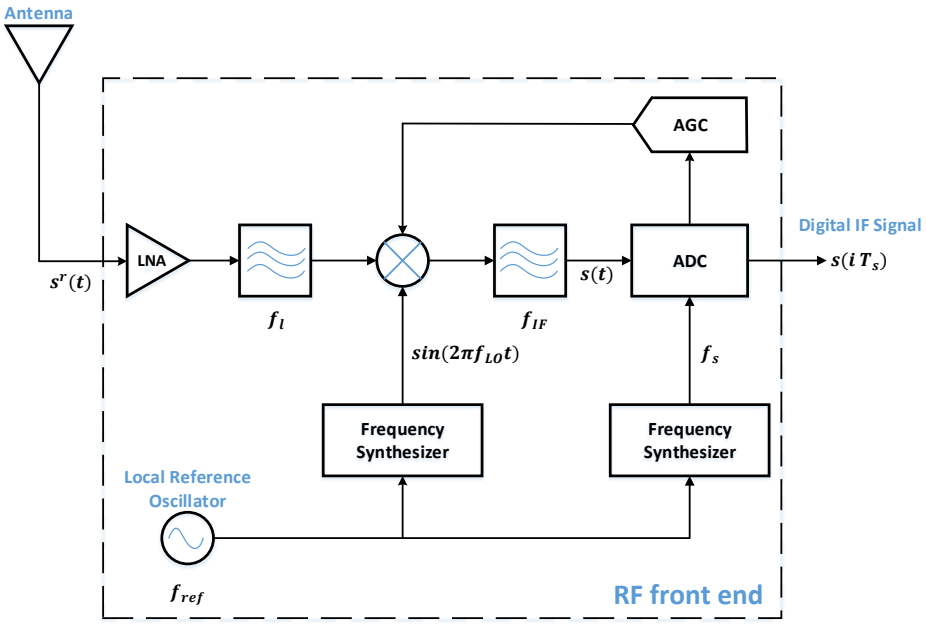

Fig. 1: RF front end of a GNSS receiver. In the RF front end, the signal $s^r(t)$ sensed by the GNSS antenna is amplified using a Low Noise Amplifier before being regulated by the Automatic Gain Control. Then, using a Frequency Synthesizer, the received signal is down converted with a local oscillator frequency f_{LO} to an intermediate frequency f_{IF}. Finally Analog-to-Digital Conversion is applied to the down-converted signal $s\,(t)$ with a sampling frequency f_s to obtain the digital signal $s\,(i\,T_s)$.

A front end processes an in-phase component and a quadrature component of the received signal with local replicas. In practice, the GNSS receivers are numerical, therefore the local replicas generated at the receiver are digitized. These local replicas are defined for a satellite v by the following expressions :

$$ci_{v,i} = CA_v(t_i + \tau_v) \sin(2\pi f_v\, t_i + \phi_v) \tag{2}$$
$$cq_{v,i} = CA_v(t_i + \tau_v) \cos(2\pi f_v\, t_i + \phi_v) \tag{3}$$

Where t_i is the time instant associated to the sampling frequency f_s and τ_v is the code delay. f_v and ϕ_v are respectively the frequency and the phase delay of the carrier. In modernized GNSS signals, there is a primary PRN code in addition to a secondary code or/and a sub-carrier. To use the proposed method in such cases, the message of navigation and the secondary code should be removed. Otherwise, the pilot channel of the

signal can be used (e.g. L5). For low frequency sub-carrier such as the Binary Offset Carrier modulation, the proposed model can be modified to take into account other PRN codes and secondary codes in the definition of the local replica and the model of the received signal. The in-phase component of correlation I_v and the quadrature component Q_v for each satellite v are obtained by integration of the sampled signals on one period of CDMA code T_b (therefore with $f_s\ T_b$ samples). Then we have :

$$I_v = \sum_{i=1}^{f_s\ T_b} s_i\ ci_{v,i} \tag{4}$$

$$Q_v = \sum_{i=1}^{f_s\ T_b} s_i\ cq_{v,i} \tag{5}$$

Assuming that $\tau_v^r = \tau_l$, $f_v^r = f_l$, $\phi_v^r = \phi_l$, we can derive the following expressions :

$$I_v = \frac{K\ A_v\ f_s\ T_b}{2} + K\ \eta_v^I \tag{6}$$

$$Q_v = K\ \eta_v^Q \tag{7}$$

where η_v^I and η_v^Q are random noises distributed according to a centered Gaussian distribution of variance $\frac{f_s\ T_b}{2}$. In this context, a classical definition of the SNR is given by :

$$SNR = \left(\frac{mean(I_v)}{std(Q_v)}\right)^2 = \frac{A_v^2\ f_s\ T_b}{2} \tag{8}$$

Where *std* and *mean* are respectively the standard deviation and mean estimates. We observe that the SNR is proportional to the square of the amplitude of the signal and independent of K, the AGC Gain. This is the reason why the SNR is used as an observation of the signal amplitude.

2.2. GNSS one bit front end model

In a GNSS receiver front end, the ADC quantizes the signal in order to map the infinite number of sampled signals to a smaller set after digitization [21]. In our approach, 1-bit quantization is applied. We show in figure 2, the processing block diagram of the in-phase component in a GNSS receiver front end. We show in figure 3, the principle of the Analog to Digital Conversion (ADC).

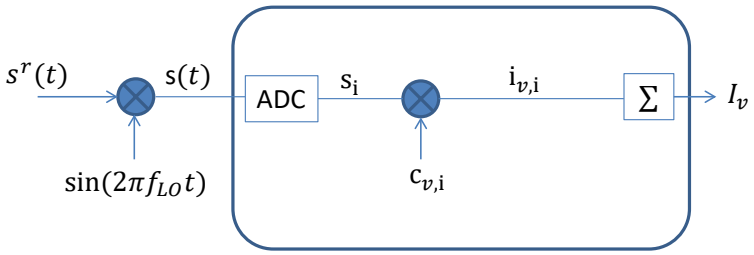

Fig. 2: Radio frequency GNSS receiver block diagram.

The expressions of the signals in figure 2 are defined after digitization by:

$$s_i = \left\lfloor \sum_{l \in V} A_l CA_l(t_i + \tau_l) \sin(2\pi f_l\ t_i + \phi_l) + \eta_i \right\rfloor_{>0} \tag{9}$$

$$c_{v,i} = \lfloor CA_v(t_i + \tau_v) \sin(2\pi f_v\ t_i + \phi_v) \rfloor_{>0} \tag{10}$$

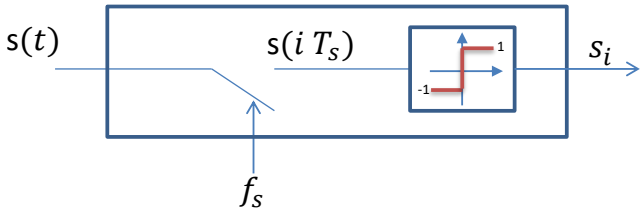

Fig. 3: Analogic to Digital Conversion (ADC) with 1-bit of quantization.

where s_i and $c_{v,i}$ are respectively the digitized signal and local replica. $\lfloor \ldots \rfloor_{>0}$ is a sign function that associates -1 to the negative values of the signal and +1 to positive (or zero) values.

Our aim is to derive an expression that links the amplitude A_v of the received signal to the mean value of the in-phase component. In this context, we define $i_{v,i} = s_i\, c_{v,i}$ to take the value +1 when s_i is equal to $c_{v,i}$ and -1 when they are different. Let's define the mean value of $i_{v,i}$ as:

$$\begin{aligned} E(i_{v,i}) &= \sum_{x\in\{-1,1\}} x\, P(i_{v,i} = x) \\ &= 2\, P(i_{v,i} = 1) - 1 \end{aligned} \tag{11}$$

where $P(i_{v,i} = x)$ is the probability of $i_{v,i} = s_i\, c_{v,i}$ to take the value x. In our GNSS front end model, the noisy samples $i_{v,i}$ are integrated on one period of CDMA code T_b. Assuming that the random values of $i_{v,i}$ are independent, we derive the mean value of I_v as follows:

$$E(I_v) = E(i_{v,i})\, T_b f_s \tag{12}$$

where $T_b f_s$ is the number of samples integrated over one period of code. $E(I_v)$ is defined by the probability $P(i_{v,i} = 1)$. We show in section 4.1 that this probability is a function of A_v.

3. Kalman estimate of the signal amplitude

In our approach, we develop an on-line estimate of the amplitudes of GNSS signals. For this purpose, we construct a state estimate that uses the in-phase components of correlation as observations. The observations $I_{v,k}$, are processed by the receiver at instant k every period of code T_b. The state model is a classical second order state equation used for data smoothing where the second state is the rate of change of the first state.

For a satellite l in the set V of visible satellites, $A_{l,k}/l \in V$ are the amplitudes of the received GNSS signals. We assume that the amplitudes are constant during one period T_b of the CDMA code. Let $n = Card\,\{V\}$ be the number of visible satellites. We consider n observations $I_{V,k}$ of the in-phase component at each instant k. The aim is to estimate the n amplitudes $A_{V,k}$ with the n observations $I_{V,k}$. We show that this problem is non-linear because expression (12) that links these two sets of values is non-linear.

The rate of change of $A_{l,k}$ is denoted as $\dot{A}_{l,k}$. We consider the following linear state equation for each satellite l:

$$A_{l,k} = A_{l,k-1} + T_b \dot{A}_{l,k-1} + \nu_{1,k} \tag{13}$$

$$\dot{A}_{l,k} = \dot{A}_{l,k-1} + \nu_{2,k} \tag{14}$$

The gaussian noises $\nu_{1,k}$, $\nu_{2,k}$ represent the model errors. They are respectively the state noise error on the amplitude and the state noise error on the variations of the amplitude. The non-linear measurement equation is defined by :

$$I_{v,k} = f\left(\{A_{l,k}\}_{l\in V}; \{\theta_{l,k}\}_{l\in V}\right) + \omega_k \tag{15}$$

where $f(...)$ is defined by expression (12) and ω_k is a Gaussian noise of variance R. $\theta_{l,k} = \{\hat{\tau}_{l,k}, \hat{f}_{l,k}, \hat{\phi}_{l,k}\}$ denotes the GNSS signal parameters provided by the PLL (Phase Lock Loop) and DLL (Delay Lock Loop) components of the receiver. The receiver architecture principle is presented in figure 4.

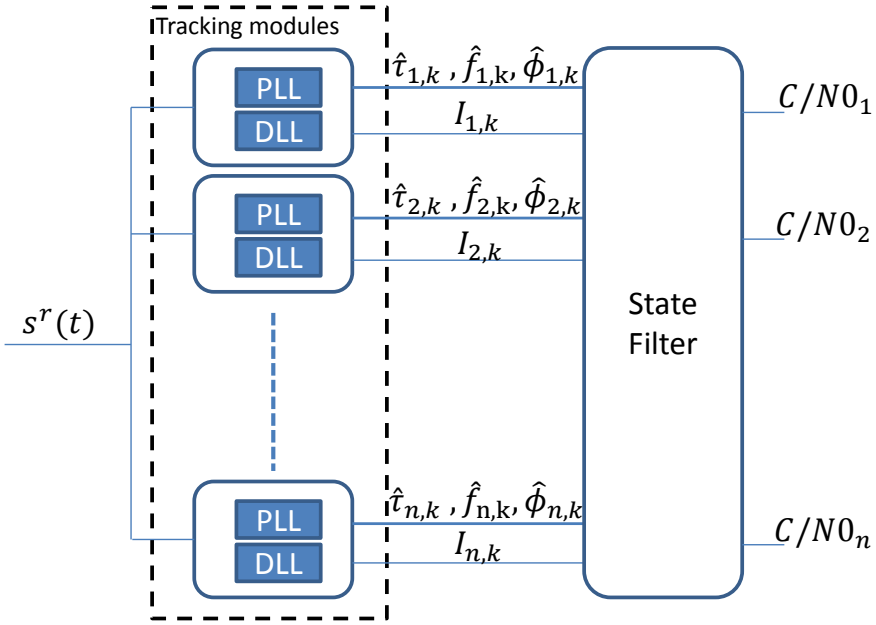

Fig. 4: Implementation of the proposed estimate in a GNSS receiver. In this implementation, the signal received by each satellite in view is tracked by a Delay Lock Loop and a Phase Lock Loop. This tracking module provides, for each satellite, observations of the code delay, phase, Doppler frequency and the in-phase component I which are used as an input to the state filter. The EKF (state filter) processes these observations to estimate the carrier-to-noise ratio of each satellite.

In this article, we propose to implement the state filter as an extended Kalman filter. This filter is derived with a local linearization of the measurement equation.

4. Linearization of the measurement equation

4.1. Statistical front end model

The probability for the random variable $i_{v,k}$ to take the value +1 is a function of the values of the local code and the received signal. These two signals sampled and quantified on one bit take the values +1 or -1. This probability is expressed as:

$$P(i_{v,i} = 1) = P(c_{v,i} = 1)\,P(s_i = 1/c_{v,i} = 1) + P(c_{v,i} = -1)\,P(s_i = -1/c_{v,i} = -1) \tag{16}$$

where $i_{v,k}$ the product of s_i with $c_{v,i}$ is equal to one in both cases. Let us construct the following model approximation of the sampled signal of satellite v after digitization:

$$\hat{s}_i = \sum_{l \in V} A_l CA_l(t_i + \hat{\tau}_l) \sin(2\pi \hat{f}_l \, t_i + \hat{\phi}_l) \tag{17}$$

$$s_i \approx \lfloor \hat{s}_i + \eta_i \rfloor_{>0} \tag{18}$$

and

$$c_{v,i} \approx \left\lfloor CA_v(t_i + \hat{\tau}_v) \sin(2\pi \hat{f}_v \, t_i + \hat{\phi}_v) \right\rfloor_{>0} \tag{19}$$

In practice, the estimates $\hat{\tau}_l$ and $\hat{f}_l, \hat{\phi}_l$ are respectively provided by the DLL and the PLL of the GNSS receiver presented in figure 4. In this model approximation, it is assumed that $\hat{\tau}_l = \hat{\tau}_v$, $\hat{f}_l = \hat{f}_v$ and $\hat{\phi}_l = \hat{\phi}_v$ in order to obtain the maximum of correlation. Therefore, A_l is the parameter to estimate. Expression (16) can be written as :

$$P\left(i_{v,i} = 1\right) = P\left(c_{v,i} = 1\right) P\left(\eta_i \geq -\hat{s}_i / c_{v,i} = 1\right) + P\left(c_{v,i} = -1\right) P\left(\eta_i < -\hat{s}_i / c_{v,i} = -1\right) \tag{20}$$

The probabilities in expression (16) can then be derived as:

$$P\left(c_{v,i} = -1\right) = \frac{\sum_{i=1}^{f_s T_b} \left| c_{v,i} - 1 \right|}{2 f_s T_b} \tag{21}$$

$$P\left(c_{v,i} = 1\right) = 1 - P\left(c_{v,i} = -1\right) \tag{22}$$

$$= \frac{\sum_{i=1}^{f_s T_b} \left(c_{v,i} + 1 \right)}{2 f_s T_b} \tag{23}$$

An estimate of the first probability of expression (20) associated to the additive random noise on the signal is defined as:

$$P\left(\eta \geq -\hat{s}_i / c_{v,i} = 1\right) = \frac{2}{\sum_{i=1}^{f_s T_b} \left(c_{v,i} + 1 \right)} \sum_{\{\tilde{i}\}_v^1} P(\eta \geq -\hat{s}_i) \tag{24}$$

where the set $\{\tilde{i}\}_v^1$ defines the values of the index i as $i / c_{v,i} = 1$. The noise is assumed to be distributed according to a Gaussian density with a unit variance. The probability $P(\eta \geq -\hat{s}_i)$ is processed with the tabulated error function as follows:

$$\sum_{\{\tilde{i}\}_v^1} P(\eta \geq -\hat{s}_i) = \sum_{\{\tilde{i}\}_v^1} \int_{-\hat{s}_i}^{+\infty} \frac{1}{\sqrt{2\pi}} exp(\frac{-x^2}{2}) \, dx$$

$$= \sum_{\{\tilde{i}\}_v^1} \frac{1}{2} erfc\left(\frac{-\hat{s}_i}{\sqrt{2}} \right) \tag{25}$$

The second probability estimate of expression (20) associated to the additive random noise on the signal is defined as:

$$P\left(\eta < -\hat{s}_i / c_{v,i} = -1\right) = 1 - \frac{2}{\sum_{i=1}^{f_s T_b} \left| c_{v,i} - 1 \right|} \sum_{\{\tilde{i}\}_v^2} P(\eta \geq -\hat{s}_i) \tag{26}$$

where the set $\{\tilde{i}\}_v^2$ defines the values of the index i as $i/c_{v,i} = -1$. For a set of estimates $\{\hat{\tau}_l, \hat{f}_l, \hat{\phi}_l\}_{l \in V}$ the probability of expression (20) is a function of $\{\hat{A}_l\}_{l \in V}$. In this context, the mean value of I_v is a function of A_v.

4.2. Derivation of the linearized measurement equation

According to equations (11), (12) , and (20) we derive the following expression :

$$\begin{aligned} f\left(\{A_{l,k}\}_{l \in V}; \{\theta_{l,k}\}_{l \in V}\right) &= 2T_b f_s \, P\left(c_{v,i} = 1\right) P\left(\eta \geq -\hat{s}_i / c_{v,i} = 1\right) \\ &+ 2T_b f_s \, P\left(c_{v,i} = -1\right) P\left(\eta < -\hat{s}_i / c_{v,i} = -1\right) - T_b f_s \end{aligned} \tag{27}$$

Considering that the values of I_v are obtained at instants k, the preceding expression can be written as below after simplification :

$$f\left(\{A_{l,k}\}_{l \in V}; \{\theta_{l,k}\}_{l \in V}\right) = \sum_{\{\tilde{i}\}_{v,k}^1} erfc\left(\frac{-\hat{s}_i}{\sqrt{2}}\right) - \sum_{\{\tilde{i}\}_{v,k}^2} erfc\left(\frac{-\hat{s}_i}{\sqrt{2}}\right) + \sum_{i=1}^{f_s T_b} \left| c_{v,i} - 1 \right| - T_b f_s \tag{28}$$

The GPS signal is very weak, so the values of $\hat{s}_i$ are small. Therefore, the following approximation (the first order of the Taylor Series expansion at zero) of the tabulate function can be used:

$$erfc(x) \approx 1 - \frac{2}{\sqrt{\pi}} x \tag{29}$$

In this context, an approximation of the function $f(...)$ is given as :

$$\begin{aligned} f\left(\{A_{l,k}\}_{l \in V}; \{\theta_{l,k}\}_{l \in V}\right) \approx & \frac{\sum_{i=1}^{f_s T_b} (c_{v,i} + 1)}{2} + \frac{2}{\sqrt{2\pi}} \sum_{\{\tilde{i}\}_{v,k}^1} \hat{s}_i \\ - & \frac{\sum_{i=1}^{f_s T_b} \left| c_{v,i} - 1 \right|}{2} - \frac{2}{\sqrt{2\pi}} \sum_{\{\tilde{i}\}_{v,k}^2} \hat{s}_i \\ + & \sum_{i=1}^{f_s T_b} \left| c_{v,i} - 1 \right| - T_b f_s \end{aligned} \tag{30}$$

and after simplification :

$$f\left(\{A_{l,k}\}_{l \in V}; \{\theta_{l,k}\}_{l \in V}\right) \approx \frac{2}{\sqrt{2\pi}} \left(\sum_{\{\tilde{i}\}_{v,k}^1} \hat{s}_i - \sum_{\{\tilde{i}\}_{v,k}^2} \hat{s}_i \right) \tag{31}$$

In order to find a linear expression between $I_{v,k}$ and $A_{v,k}$ we develop the expression of $\hat{s}_i$:

$$f\left(\{A_{l,k}\}_{l\in V};\{\theta_{l,k}\}_{l\in V}\right) \approx \frac{2}{\sqrt{2\pi}}\left(\sum_{l\in V} A_{l,k}\left(\sum_{\{\tilde{i}\}^1_{v,k}} CA_l(t_i+\hat{\tau}_{l,k})\sin(2\pi\hat{f}_{l,k}\,t_i+\hat{\phi}_{l,k})\right.\right.$$
$$\left.\left. - \sum_{\{\tilde{i}\}^2_{v,k}} CA_l(t_i+\hat{\tau}_{l,k})\sin(2\pi\hat{f}_{l,k}\,t_i+\hat{\phi}_{l,k})\right)\right) \tag{32}$$

Finally, for a set V of n satellites in view we have the following linear expression :

$$I_{V,k} \approx HA_{V,k} + \omega_k \tag{33}$$

with $I_{V,k} = [I_{1,k},\ldots,I_{n,k}]^T$ and $A_{V,k} = [A_{1,k},\ldots,A_{n,k}]^T$. The expression of an element $h_{i,j}$ of H, is given by :

$$h_{v,l} = \frac{2}{\sqrt{2\pi}}\left(\sum_{\{\tilde{i}\}^1_{v,k}} CA_l(t_i+\hat{\tau}_{l,k})\sin(2\pi\hat{f}_{l,k}\,t_i+\hat{\phi}_{l,k})\right.$$
$$\left. - \sum_{\{\tilde{i}\}^2_{v,k}} CA_l(t_i+\hat{\tau}_{l,k})\sin(2\pi\hat{f}_{l,k}\,t_i+\hat{\phi}_{l,k})\right) \tag{34}$$

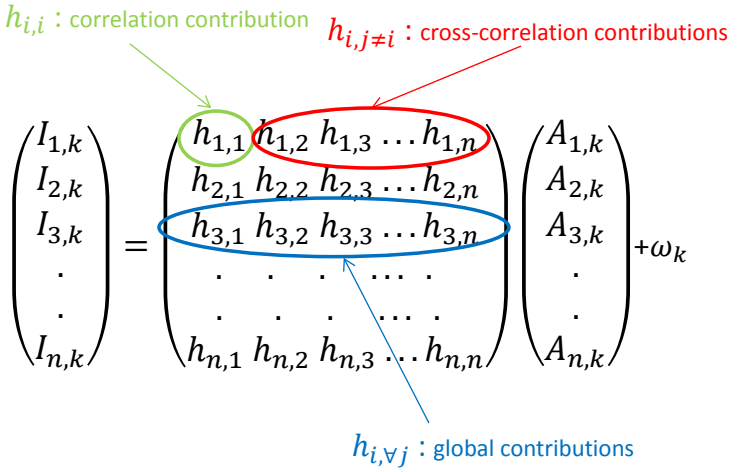

Fig. 5: Contribution of each satellite in the observations $I_{v,k}$. Each element $h_{i,j}$ of H is processed using equation (34), where the set $\{\tilde{i}\}^1_v$ defines the values of the index i as $i/c_{v,i} = 1$, and the set $\{\tilde{i}\}^2_v$ defines the values of the index i as $i/c_{v,i} = -1$. For a component $I_{i,k}$, $h_{i,i}$ is the correlation contribution of the signal from satellite i and $h_{i,j}$ is the inter correlation contribution of the signal from satellite j.

We present in figure 5 the different elements of H. In this matrix, we note the cross-correlation contributions and the correlation contributions in the observations $I_{v,k}$ for each satellite. The component $h_{i,j}$ represents the contribution of satellite j when a replica of the signal of satellite i is used to demodulate and demultiplex the signal. In this context, for a component $I_{i,k}$, $h_{i,i}$ is the correlation contribution of the signal from satellite i and $h_{i,j}$ is the inter correlation contribution of the signal from satellite j. We define the cross-correlation contribution $\mathbf{h}_{i,j\neq i} = \sum_{j\neq i} h_{i,j}$ and the global contribution $\mathbf{h}_{i,\forall j} = \sum_{j=1}^{n} h_{i,j}$. One of the interests of the proposed approach is to study the effect of the cross-correlation contribution on the estimation. We show by experimentation the impact of this contribution on the accuracy of the estimated amplitudes of GNSS signals.

5. Experimentation

5.1. Assessment on synthetic data

The aim of this experimentation is to assess the proposed amplitudes estimator on GPS C/A signals and study the effect of the correlation contribution on the carrier-to-noise estimation. In order to be independent of the AGC Gain, we compare the carrier-to-noise ratio in dB-Hz using the below expressions derived from the classical definition of the SNR in equation (8):

$$C/N_0^k = 20\log\left(\frac{A_v\ \sqrt{f_s\ T_b}}{\sqrt{2}}\right) + 10\log(BW) \tag{35}$$

$$C/N_0^c = 20\log\left(\frac{mean(I_{v,k=1:1000})}{std(I_{v,k=1:1000})}\right) + 10\log(BW) \tag{36}$$

Where C/N_0^k is the carrier-to-noise equation used in our approach, and C/N_0^c is a classical carrier-to-noise definition. $\frac{A_v}{\sqrt{2}}$ is the Root Mean Square voltage of the carrier and BW is the noise equivalent bandwidth of the receiver RF front end. We report in Table 1 the Doppler frequency of the visible satellites during the simulation.

Table 1: Satellites' Doppler frequencies

Satellites' PRN	Doppler Frequency f_l^D
30	-3312
28	-2422
10	2224
20	123
11	634
24	2268
19	3297
12	3987
13	-2398
15	-874
17	1873

We show in figure 6, the observations $I_{1,k}$ and $E(I_{1,k})$ for satellite PRN 12 during 1 second (k=1:1000). This means that one value of $I_{1,k}$ and $E(I_{1,k})$ is obtained every millisecond. In this experimentation, $A_{V,k}$ = 0.05 for all satellites in view and η_i, the Gaussian noise on the received signal, have a variance 1. The amplitudes of the signals are fixed to 0.05 and the noise power to 1 in order to provide a true value for the carrier-to-noise ratio of GPS C/A signals which is 43.98 dB-Hz (i.e. C/N_0^t = 43.98 db-Hz). In figure 6, we observe the evolution of $E(I_{v,k})$ due to the global correlation contribution and the random like evolution of $I_{v,k}$ due to the global correlation contribution and the noise on the received signal. We show by experimentation, that the statistics of $I_{v,k}$ and the classical SNR estimates are functions of the cross-correlation contribution.

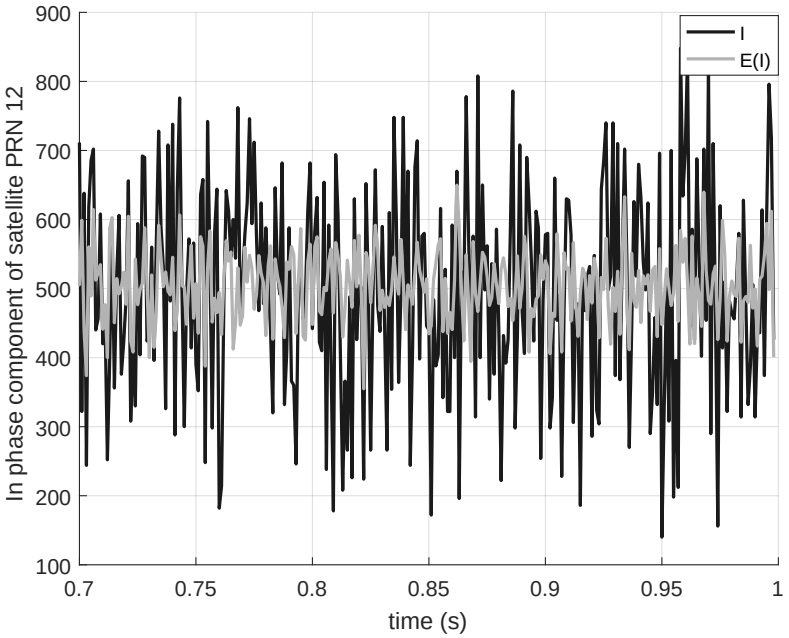

Fig. 6: Noisy observations $I_{1,1:1000}$ and $E(I_{1,1:1000})$ for satellite PRN 12

We assess the statistic of $I_{v,k}$ from the analysis of matrix H. This study is independent of the amplitudes $\{A_{l,k}\}_{l\in V}$ and of η_i the noise on the received signal. C/N_0^c is used to assess the cross-correlation contribution on the statistic of $I_{v,k}$. We report in Table 2, the standard deviation of the cross-correlation contribution $\mathbf{h}_{i,j\neq i}$ processed over different satellites for one second of observations, and the standard deviation of the contribution $h_{i,i}$ calculated for every satellite along the observation time. We also report the mean value and the standard deviation of the total contribution $\mathbf{h}_{i,\forall j} = \sum_{j=1}^{n} h_{i,j}$ processed over different satellites for one second of observations. Finally, we calculate the classical carrier-to-noise ratio C/N_0^c and the true carrier-to-noise ratio C/N_0^t obtained using equation (35) with $A_{V,1:1000} = 0.05$ for all satellites in view. In practice, the carrier frequency f_l of a down converted signal constitutes of the intermediate frequency f_l^{IF} and the Doppler frequency f_l^D where $f_l = f_l^{IF} + f_l^D$. This means that for high f_l^{IF}, the Doppler effect will be notably mitigated, and the standard deviation of the correlation contributions will be very close for every satellite. Thus, in order to study the Doppler effect on the correlation contributions, we consider that $f_l^{IF} = 0\ Hz$ and therefore, $f_l = f_l^D$. This is only applicable for assessment on synthetic data. In the real case, f_l^{IF} is always present for any GNSS receiver which hugely alters Doppler effect.

We notice in Table 2 that the mean contribution $\bar{\mathbf{h}}_{i,\forall j}$, proportional to the mean value of $I_{v,k}$, is independent of the satellites, because the values of $\bar{\mathbf{h}}_{i,\forall j}$ are indeed close. However, the standard deviations $\sigma_{\mathbf{h}_{i,\forall j}}$ of the global contribution are dependent of the satellites. The standard deviations $\sigma_{\mathbf{h}_{i,j\neq i}}$ associated to the cross-correlation contribution are close, so weakly dependent of the satellites. The dependence is due to the correlation contribution of each satellite defined as the standard deviation $\sigma_{h_{i,i}}$. This standard deviation is indeed a function of the Doppler frequency. For low Doppler, like satellites PRN 11 and 20 in Table 1, the standard deviation $\sigma_{h_{i,i}}$ and the standard deviation $\sigma_{\mathbf{h}_{i,\forall j}}$ of the global contribution increase notably (in bold; Table 2). Finally we observe in Table 2 that the carrier-to-noise ratio C/N_0^c and the true carrier-to-noise ratio C/N_0^t are different. The difference is due to the cross-correlation contribution of the satellites. This difference increases with the low values of the Doppler frequency, which is noticed by the very low C/N_0^c values for satellites PRN 11 and 20.

Table 2: Cross-correlation impact

Sats	$\sigma_{\mathbf{h}_{i,j\neq i}}$	$\sigma_{h_{i,i}}$	$\bar{\mathbf{h}}_{i,\forall j}$	$\sigma_{\mathbf{h}_{i,\forall j}}$	C/N_0^t (dB-Hz)	C/N_0^c (dB-Hz)
30	1054	386	10155	1125	43.98	42.75
28	1009	355	10109	1068	43.98	43.18
10	1031	467	10145	1134	43.98	42.67
20	1077	**4386**	10179	**4463**	43.98	33.41
11	988	**960**	10155	**1387**	43.98	41.58
24	918	463	10108	1036	43.98	43.1
19	938	391	10149	1015	43.98	43.46
12	1080	322	10144	1127	43.98	43.4
13	1049	374	10149	1114	43.98	42.9
15	936	704	10109	1164	43.98	42.73
17	1021	436	10126	1116	43.98	43.02

We report, in Table 3, the mean and standard deviation of the total contribution $\mathbf{h}_{i,\forall j}$ of satellite PRN 12. In this table, we show the total contribution as a function of the number of visible satellites. We also report the classical carrier-to-noise ratio C/N_0^c and the true carrier-to-noise ratio C/N_0^t. With Table 3, we conclude that the statistic of $I_{v,k}$ is a function of the number of satellites. The standard deviation $\sigma_{h_{i,\forall j}}$ indeed increases with the number of satellites and the mean value of the global contribution is nearly constant. The standard deviation is inversely proportional to C/N_0^c. The increase in the standard deviation, leads to an expected decrease in C/N_0^c. Therefore, the difference between C/N_0^c and C/N_0^t increases with the increase in the standard deviation and thus with the number of satellites. This also proves the influence of the correlation contribution of the satellites on the carrier-to-noise estimation.

Finally, we present in Table 4, the estimate C/N_0^k obtained with the proposed approach. In this case, C/N_0^k is processed with expression (35) and the estimated amplitudes are provided by the Kalman filter every 1ms. We compare C/N_0^k with the true carrier-to-noise ratio C/N_0^t to prove the accuracy of the proposed approach. In Table 4, R and Q are the covariance matrix of the measurements and state noises respectively. Columns 3 and 4 show respectively, the mean estimate and the standard deviation of the carrier-to-noise ratio when the observations are not smoothed by the filter. In columns 5 and 6, we report the same parameters when the observations are smoothed by the filter. Since I are noisy observations, the choice of the Kalman filter parameters is important for the accuracy of the estimate. In our approach, we determine the values of R and Q with the observations and the estimations. In this regard, we determine a fixed value of R with the measurements of the noise on the observations of the in-phase component of the signal. However, the tuning of Q is dependent on the application and must be done according to the constraints of this application. The value of Q is determined while taking into consideration that there is a trade-off between the accuracy of the estimation and the ability to follow the changes in the observations. In our approach, we fix R and tune the value of Q to obtain the same accuracy as the NovAtel GNSS receiver, which is a widely known commercial scientific GNSS receiver. In fact, the information provided by the NovAtel GNSS receiver is used as a reference in many GNSS-R applications. Based on the forgoing, we choose for our application a high covariance matrix of the measurement R and a small covariance of the process noise Q because the variations in the signal amplitude are low. For this experimentation, R=10,000,000,000 and Q=0.05.

Table 3: The impact of the number of satellites

Number of satellites	Visible satellites PRN	$\sigma_{h_{i,\forall j}}$	$\bar{\mathbf{h}}_{i,\forall j}$	C/N_0^t (dB-Hz)	C/N_0^c (dB-Hz)
1	12	322	10149	43.98	43.69
2	12,17	467	10148	43.98	43.64
3	12,17,19	545	10149	43.98	43.51
4	12,17,19,13	687	10149	43.98	43.46
5	12,17,19,13,24	756	10148	43.98	43.42
6	12,17,...,24,28	829	10149	43.98	43.35
7	12,17,...,28,10	941	10149	43.98	43.22
8	12,17,...,10,15	995	10149	43.98	43.16
9	12,17,...,15,11	1034	10148	43.98	43.12
10	12,17,...,11,20	1085	10144	43.98	42.98
11	12,17,...,20,30	1127	10144	43.98	42.84

Table 4: Estimated carrier-to-noise ratio

$C/N0$ (dBHz) Sats	C/N_0^t	C/N_0^k $R = Q$		C/N_0^k $R >> Q$	
		mean	std	mean	std
30	43.98	43.32	3.01	43.85	0.24
28	43.98	43.57	2.72	43.92	0.22
10	43.98	43.52	2.97	43.99	0.24
20	43.98	43.37	6.03	43.88	0.26
11	43.98	43.4	3.31	43.99	0.18
24	43.98	43.55	2.75	43.91	0.32
19	43.98	43.52	2.82	43.98	0.22
12	43.98	43.31	2.86	43.91	0.19
13	43.98	43.56	2.77	43.92	0.24
15	43.98	43.57	2.86	43.97	0.24
17	43.98	43.72	2.78	44.01	0.25

From Table 4, we notice that the carrier-to-noise estimate C/N_0^k does not depend on the satellite, so its computation removes the cross-correlation error. This can be clearly seen by comparing the mean of C/N_0^k in columns 3 and 6 with C/N_0^c in Table 2 for satellites PRN 11 and 20 obtained with 1000 samples of I.

By comparing, columns 3 and 4 with columns 5 and 6, we show that the proposed filter smooths the estimate and improves its accuracy. The values of the mean of C/N_0^k in column 6 are indeed closer to the true carrier-to-noise ratio C/N_0^t. From the preceding, we can conclude that the proposed approach can remove the error due to the cross-correlation contribution and improve the accuracy of the carrier-to-noise ratio estimate.

In addition, by decreasing the number of I samples used to calculate C/N_0^c from 1000 to 800 samples among the satellites v, we noticed that our approach which is based on the on-line estimate of C/N_0^k every 1ms, can achieve the same accuracy as the classical estimate C/N_0^c obtained with 800 samples of the in-phase component for each satellite v, when the observations are smoothed by the Kalman filter (i.e. R=10,000,000,000 and Q=0.05). In addition, we conclude that the proposed approach has the advantage of following the evolution of the mean in a much higher accuracy, due to the fact that our approach provides an estimate of the carrier-to-noise ratio each 1ms.

5.2. Assessment on real data

The experiment started at 15h20 UTC the 13^{th} of December 2019 and lasted for 1 minute. A NovAtel GNSS-850 antenna was mounted on the top of the LISIC laboratory building at (50.953228°N; 1.880285°E). In this experiment, a NovAtel OEM7 receiver was used to provide RINEX observation and navigation files. The observation file contains data such as the total number of satellites in view at each instant, the PRN codes of the satellites, and the carrier-to-noise ratio for each signal at different instants. A Syntony Echo-L bit-grabber was used to digitize the received signals. This experimentation is dedicated to the use of GPS C/A signals. We present in figure 7, the experimental setup.

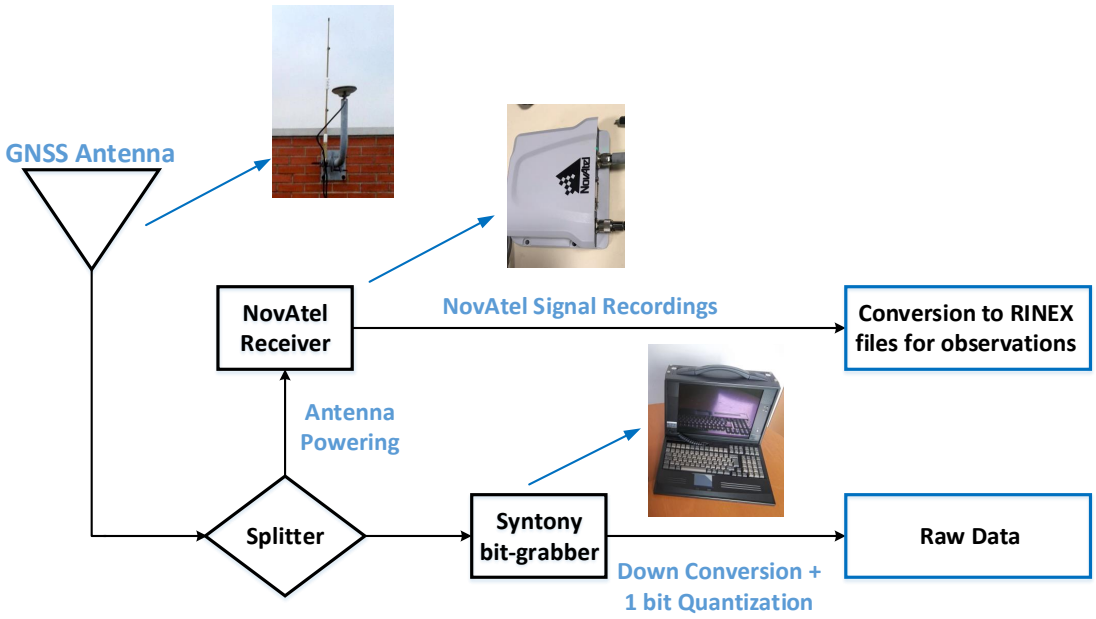

Fig. 7: Experimental setup showing the connections between the various elements and its roles. The GNSS antenna, powered by the NovAtel receiver, captures signals from all the satellites in view. Then, the received signals enter a splitter and are passed to the NovAtel receiver and to the Syntony bit-grabber. Using the NovAtel signal recordings, RINEX files are generated from which the carrier-to-noise ratio provided by the NovAtel receiver can be retrieved. On the other hand, the Syntony bit-grabber digitizes the received signals with down conversion and 1-bit quantization to provide raw data, which are processed to estimate the carrier-to-noise ratio.

The data collected by the NovAtel receiver and the raw data provided by the Sytnony bit-grabber are not synchronized. Therefore, data synchronization is applied. In this regard, the received signals have sev-

eral essential components to be identified: the carrier frequency, the PRN code unique to each satellite, the code delay, the phase delay, and the navigation message from which the GPS time and pseudo-range can be retrieved [22]. In order to recover these components and date the signals for synchronization, signal acquisition and tracking are implemented. As a result, the message of navigation is extracted, which is then used for signal dating.

The message of navigation provides timing information that allows to calculate the seconds of the GPS week, which constitute the GPS time along with the GPS week number [23]. Then using the estimated GPS time of the digitized signals and the GPS time of the signals provided by the RINEX observation file, data synchronization is applied for assessment of the proposed approach.

The assessment of the proposed GNSS signal amplitude estimator which uses a 1-bit quantization GNSS receiver, is realized by comparing the carrier-to-noise ratio C/N_0^k obtained with the proposed approach and the carrier-to-noise ratio C/N_0^r provided by the RINEX observation file for each satellite v via the NovAtel GNSS receiver. As in the synthetic case, we calculate the estimated C/N_0^k using equation (35), where the amplitudes of the signals are provided by the Kalman filter every 1ms. In this experimentation, the observations are smoothed by the Kalman filter with R=10,000,000,000 and Q=0.0001. We present in figure 8, a sky plot of the satellites constellation which shows the positions of the satellites as recorded by the NovAtel receiver.

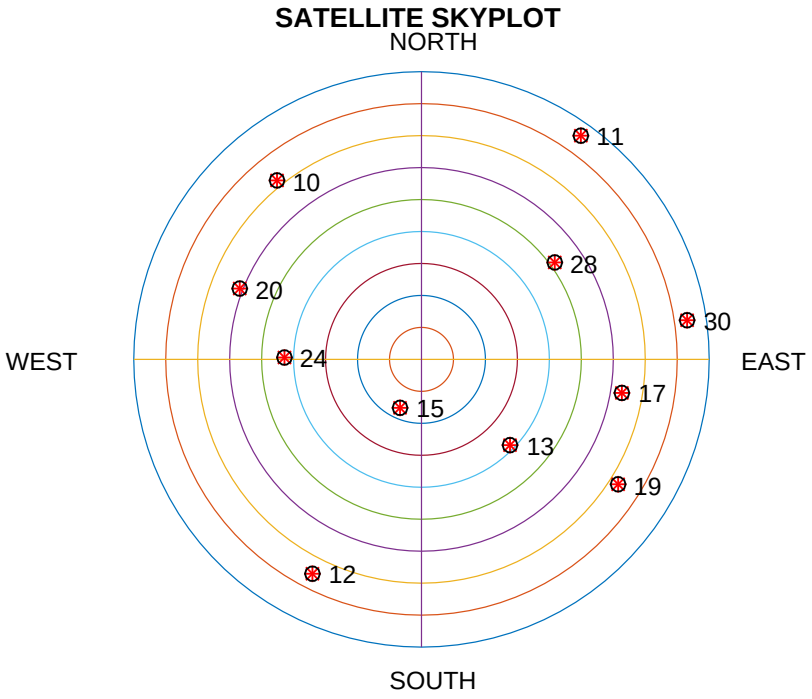

Fig. 8: Constellation of the visible GPS satellites as recorded by the NovAtel receiver

We show in figure 9, the C/N_0^r provided by the NovAtel receiver every 1 second and the C/N_0^k estimated by the proposed approach every 1ms for different satellites (satellites PRN 19,28,12 and 15). We also report the 1ms rate carrier-to-noise observations C/N_0^o obtained using the amplitudes derived from equation (33).

The obtained results show good agreement between the carrier-to-noise ratio C/N_0^r provided by the NovATel GNSS receiver and C/N_0^k estimated by our approach. For satellite PRN 19, where C/N_0 is relatively low and its rate of change is approximately steady, the evolution of C/N_0^k estimated by our model every 1ms fits accurately the evolution of C/N_0^r provided by the NovAtel receiver every 1s. The same observation can be deduced from satellites PRN 28 and 12, where the evolution of our model estimate is coherent with the evolution of the C/N_0^r even in the case of fast and abrupt changes in the carrier-to-noise observations as in satellite PRN 12. This also show our model's ability to track fast evolutions of the carrier-to-noise observations precisely. However, it can be observed from satellite PRN 15, that for high C/N_0 environments ($\gtrapprox$ 54 dB-Hz), our model doesn't perfectly fit the evolution of C/N_0^r. This is due to the fact that in high C/N_0 environments, the proposed non-linear model doesn't fit the *erfc* function which performs generally on low and moderate values. This results in our model being less accurate for high C/N_0 environments.

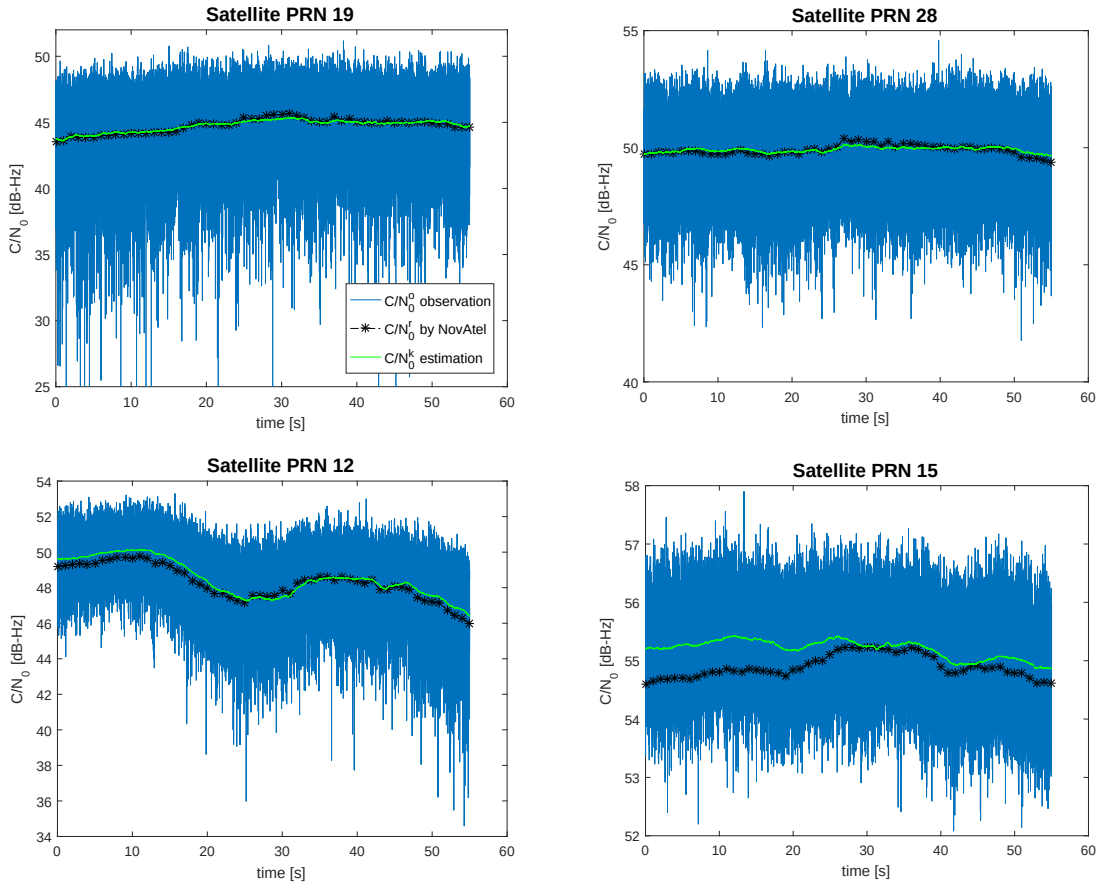

Fig. 9: C/N_0 estimation assessment. In this figure, C/N_0^r is the carrier-to-noise ratio provided by the NovAtel receiver every 1 second, C/N_0^k is the carrier-to-noise ratio estimated by the proposed approach every 1ms and C/N_0^o is the 1ms rate carrier-to-noise observations obtained using the amplitudes derived from equation (33). Note that the intervals of the ordinate axes are not fixed in the figures presented.

We present in Table 5, C/N_0^r provided by the NovATel receiver and the mean ($\overline{C/N_0^k}$) of the carrier-to-noise estimates C/N_0^k provided by the Kalman filter every 1ms. In this experimentation, we assess the mean $\overline{C/N_0^k}$ over 1 second of estimation to align with the rate of observation provided by the NovAtel GNSS receiver. The mean values $\overline{C/N_0^k}$ calculated over 1 second of estimation are indeed very close to C/N_0^r provided by the NovAtel receiver for different satellites and at different instances of time.

Table 5: Carrier-to-noise ratio mean estimation assessment

	t= 5 sec		t=25 sec		t= 50 sec	
Sats	C/N_0^r	$\overline{C/N_0^k}$	C/N_0^r	$\overline{C/N_0^k}$	C/N_0^r	$\overline{C/N_0^k}$
10	44.93	44.90	47.05	47.13	47.94	48.14
11	41.65	41.48	40.71	39.80	41.72	41.31
12	49.23	49.63	47.66	47.87	48.02	48.26
13	51.99	52.28	52.11	52.20	51.85	51.64
15	54.64	55.21	54.85	55.23	54.86	55.02
17	49.30	49.76	48.86	49.18	50.02	50.13
19	43.58	43.79	44.90	44.88	45.02	44.96
20	45.83	46.13	45.94	46.07	45.36	45.24
24	52.33	52.75	52.18	52.54	52.04	52.18
28	49.74	49.78	49.74	49.83	49.95	50.03
30	46.29	45.95	44.34	43.70	38.60	36.91

Therefore, we conclude that our approach, which uses a 1-bit quantization GNSS receiver can provide the same accuracy as the NovAtel GNSS receiver. However, it is important to note that the proposed model provides C/N_0 estimations at a much higher rate (1000 Hz) than the NovAtel GNSS receiver (1 Hz), which is proven to be crucial in multipath, and dynamic GNSS-Reflectometry applications, where the C/N_0 estimation rate defines the rate at which the environment can be analyzed.

This paper proposes a low complexity estimate with low computational load, as a trade off with the accuracy of our estimate. Nowadays, the computational power of the GNSS receiver is high and thus, complexity and computational load are no more problems. Therefore, in order to prove our estimate's ability to cope with rapid and abrupt changes encountered in multipath and dynamic GNSS-R applications, we compare the proposed estimate with an accurate C/N_0 estimate provided by Beaulieu's method presented in the literature review of the introduction. We show in figure 10, C/N_0^k estimated by the proposed approach every 1ms and C/N_0^{BL} estimated by Beaulieu's method (see equation (6) in [14]) every 100ms. We also report the 1ms rate carrier-to-noise observations C/N_0^o with abrupt changes in the amplitude measurements. This abrupt change was implemented with the aid of an attenuator designed by HP (8494A Attenuator). The attenuator was set to 1dB for 1 second to simulate the change. In this experiment, the parameters of the Kalman filter are set to R=10,000,000,000 and Q=0.0001. The abrupt change is detected by our approach through the innovation of the Kalman filter. In this context, whenever an abrupt change is detected, the Kalman filter is re-initialized and the next measurement is used as the current state.

From figure 10a, we notice that the C/N_0^{BL} estimates provided by Beaulieu's method every 100ms, have a higher variance than C/N_0^k estimates provided by our approach every 1ms. Furthermore, zooming in (figure 10b) on the part where the abrupt change in the observations has took place, we notice that C/N_0^k follows this change more accurately and rapidly than Beaulieu's method. This experimentation shows that there is a tradeoff between accuracy and capacity to follow a rapid change with respect to Beaulieu's method. The trade-off is less critical with respect to the proposed estimate that can be easily adapted to change point estimation. This further proves our estimate's ability to cope with rapid and abrupt changes

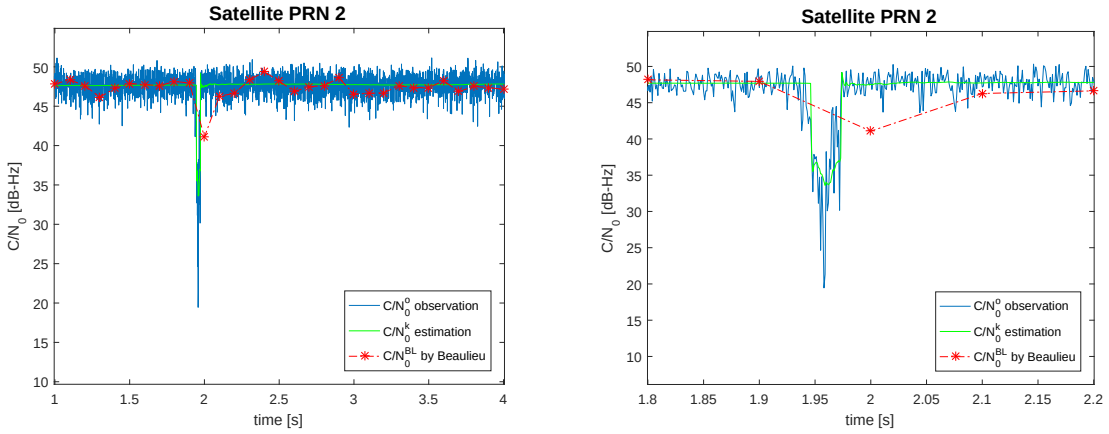

(a) (b)

Fig. 10: C/N_0 estimation assessment with abrupt changes. In this figure, C/N_0^k is the carrier-to-noise ratio estimated by the proposed approach every 1ms, C/N_0^{BL} is the carrier-to-noise ratio estimated by Beaulieu's method every 100ms, and C/N_0^o is the 1ms rate carrier-to-noise observations.

in the observations and ensures the importance of high rate C/N_0 estimations in multipath and dynamic GNSS-R applications.

6. Conclusion

In this article, we proposed an on-line estimate of the amplitudes of GNSS signals in the form of an Extended Kalman Filter that uses the 1ms rate of the in-phase components of the signals as observations. In order to be independent of the automatic gain control, 1-bit quantization digital receiver was used. The estimated amplitudes of the signals provide direct observations of C/N_0, therefore the carrier-to-noise ratio is estimated. This estimator can provide robust amplitude values and, consequently C/N_0 estimations at a high rate of 1000 Hz. We assess the performance of the estimator using synthetic and real data. In the synthetic case, we show that the proposed approach can remove the error due to the cross-correlation contribution and improve the accuracy of the carrier-to-noise estimate when the data are smoothed by the filter. We also show, in real experimentation, that the proposed estimator, which uses a 1-bit quantization receiver, performs coherently with the widely known NovAtel receiver. It was also noted that the proposed approach performs at a much higher rate than the NovAtel GNSS receiver. We also proved, using real data, our method's ability to cope with the abrupt changes in observations. This was done by comparing our estimate with an accurate C/N_0 estimate, namely Beaulieu's estimate, in the presence of abrupt changes in the observations. The experimentation showed that there is a tradeoff between accuracy and capacity to follow a rapid change with respect to Beaulieu's method, which is less critical with respect to the proposed estimate that can be easily adapted to change point estimation. The model studied in this paper can be applied on dynamic GNSS-R applications in order to derive some characteristics of the reflective surface (such as height, or soil moisture). In this context, it is crucial to obtain C/N_0 at very high rates to cope with the rapid displacement of the dynamic GNSS receiver.

Acknowledgment

The authors would like to acknowledge the Université du Littoral Côte d'Opale (ULCO) and the National Council for Scientific Research of Lebanon (CNRS-L) for granting a joint doctoral fellowship to Mr. Hamza Issa.

The authors would also like to thank the CPER MARCO project (Recherche marine et littorale en Côte d'Opale, des milieux aux ressources, aux usages et à la qualité des produits de la mer) for their financial support.

References

[1] J. W. Betz, K. R. Kolodziejski, Generalized theory of code tracking with an early-late discriminator part I: Lower bound and coherent processing, IEEE Transactions on Aerospace and Electronic Systems 45 (4) (2009) 1538–1556. doi:10.1109/TAES.2009.5310316.

[2] J. W. Betz, K. R. Kolodziejski, Generalized theory of code tracking with an early-late discriminator part II: Noncoherent processing and numerical results, IEEE Transactions on Aerospace and Electronic Systems 45 (4) (2009) 1557–1564. doi:10.1109/TAES.2009.5310317.

[3] A. A. Arroyo, A. Camps, A. Aguasca, G. F. Forte, A. Monerris, C. Rüdiger, J. P. Walker, H. Park, D. Pascual, R. Onrubia, Dual-polarization GNSS-R interference pattern technique for soil moisture mapping, IEEE Journal of Selected Topics in Applied Earth Observations and Remote Sensing 7 (5) (2014) 1533–1544.

[4] C. J. Comp, P. Axelrad, Adaptive SNR-based carrier phase multipath mitigation technique, IEEE Transactions on Aerospace and Electronic Systems 34 (1) (1998) 264–276. doi:10.1109/7.640284.

[5] S. Weaver, Z. Ucar, P. Bettinger, K. Merry, Data from: How a GNSS receiver is held may affect static horizontal position accuracy (2015). doi:doi:10.5061/dryad.8j616.
URL https://doi.org/10.5061/dryad.8j616

[6] K. M. Larson, E. E. Small, E. Gutmann, A. Bilich, P. Axelrad, J. Braun, Using GPS multipath to measure soil moisture fluctuations: initial results, GPS Solutions 12 (3) (2008) 173–177. doi:10.1007/s10291-007-0076-6.
URL https://doi.org/10.1007/s10291-007-0076-6

[7] A. Azmani, S. Reboul, J. Choquel, M. Benjelloun, Soil moisture estimation using land-reflected GPS L2C bi-static radar measurements, in: Proceedings of the 23rd International Technical Meeting of The Satellite Division of the Institute of Navigation (ION GNSS 2010), 2010, pp. 1031–1038.

[8] M. A. Ribot, J.-C. Kucwaj, C. Botteron, S. Reboul, G. Stienne, J. Leclère, J.-B. Choquel, P.-A. Farine, M. Benjelloun, Normalized GNSS interference pattern technique for altimetry, Sensors 14 (6) (2014) 10234–10257. doi:10.3390/s140610234.
URL http://www.mdpi.com/1424-8220/14/6/10234

[9] M. Troglia Gamba, G. Marucco, M. Pini, S. Ugazio, E. Falletti, L. Lo Presti, Prototyping a GNSS-based passive radar for UAVs: An instrument to classify the water content feature of lands, Sensors 15 (11) (2015) 28287–28313. doi:10.3390/s151128287.
URL http://www.mdpi.com/1424-8220/15/11/28287

[10] M. S. Grewal, L. R. Weill, A. P. Andrews, Global positioning systems, inertial navigation, and integration, John Wiley & Sons, 2007.

[11] B. W. Parkinson, J. Spilker, Global Positioning System: Theory and Applications Volume 1, American Institute of Aeronautics and Astronautics, Washington, 1996.

[12] E. Kaplan, C. Hegarty, Understanding GPS: Principles and Applications, Artech House, 2005.
URL https://books.google.fr/books?id=-sPXPuOW7ggC

[13] P. D. Groves, GPS signal-to-noise measurement in weak signal and high-interference environments, Journal of The Institute of Navigation 52 (2) (2005) 83–94.

[14] N. C. Beaulieu, A. S. Toms, D. R. Pauluzzi, Comparison of four snr estimators for qpsk modulations, IEEE communications letters 4 (2) (2000) 43–45.

[15] D. R. Pauluzzi, N. C. Beaulieu, A comparison of SNR estimation techniques for the AWGN channel, IEEE Transactions on Communications 48 (10) (2000) 1681–1691. doi:10.1109/26.871393.

[16] S. Satyanarayana, D. Borio, G. Lachapelle, C/N0 estimation: design criteria and reliability analysis under global navigation satellite system (GNSS) weak signal scenarios, IET Radar, Sonar Navigation 6 (2) (2012) 81–89. doi:10.1049/iet-rsn.2011.0164.

[17] S. Cioni, G. E. Corazza, M. Bousquet, An analytical characterization of maximum likelihood signal-to-noise ratio estimation, in: 2005 2nd International Symposium on Wireless Communication Systems, 2005, pp. 827–830. doi:10.1109/ISWCS.2005.1547825.

[18] K. Muthuraman, D. Borio, C/N0 estimation for modernized GNSS signals: Theoretical bounds and a novel iterative estimator, Journal of The Institute of Navigation 57 (4) (2010) 309–323. doi:10.1002/j.2161-4296.2010.tb01785.x.
URL http://dx.doi.org/10.1002/j.2161-4296.2010.tb01785.x

[19] G. Stienne, S. Reboul, J.-B. Choquel, M. Benjelloun, Cycle slip detection and repair with a circular on-line change-point detector, Signal processing 100 (2014) 51–63.

[20] T. J. Lim, Y. Ma, The kalman filter as the optimal linear minimum mean-squared error multiuser CDMA detector, IEEE Transactions on information theory 46 (7) (2000) 2561–2566.

[21] M. Andrianarison, New methods and architectures for high sensitivity hybrid GNSS receivers in challenging environments, Ph.D. thesis, École de technologie supérieure (2018).

[22] J. Leclère, C. Botteron, P.-A. Farine, Acquisition of modern GNSS signals using a modified parallel code-phase search architecture, Signal Processing 95 (2014) 177–191.

[23] N. I. Ziedan, GNSS receivers for weak signals, Artech house Norwood, 2006.